Title

Order-Disorder Ferroelectric Transition of Strained SrTiO3

Journal

Physical Review Letters, 125(8)

ISSN

0031-9007 1079-7114

Authors

Salmani-Rezaie, Salva
Ahadi, Kaveh
Strickland, WilliamâM.
et al.

Publication Date

2020-08-20

DOI

10.1103/PhysRevLett.125.087601

Peer reviewed

Order-Disorder Ferroelectric Transition of Strained $SrTiO_3$

Salva Salmani-Rezaie, Kaveh Ahadi, William M. Strickland, and Susanne Stemmer*
Materials Department, University of California, Santa Barbara, California 93106-5050, USA

(Received 28 December 2019; accepted 4 August 2020; published 20 August 2020)

$SrTiO_3$ is an incipient ferroelectric that is believed to exhibit a prototype displacive, soft mode ferroelectric transition when subjected to mechanical stress or alloying. We use high-angle annular dark-field imaging in scanning transmission electron microscopy to reveal local polar regions in the room-temperature, paraelectric phase of strained $SrTiO_3$ films, which undergo a ferroelectric transition at low temperatures. These films contain nanometer-sized domains in which the Ti columns are displaced. In contrast, these nanodomains are absent in unstrained films, which do not become ferroelectric. The results show that the ferroelectric transition of strained $SrTiO_3$ is an order-disorder transition. We discuss the impact of the results on the nature of the ferroelectric transition of $SrTiO_3$.

DOI: 10.1103/PhysRevLett.125.087601

The classic Devonshire model [1] of a displacive ferroelectric phase transition forms the basis of the thermodynamic theory of some of the most common ferroelectrics, such as $BaTiO_3$ [2]. It assumes that the free energy in the paraelectric phase has a single minimum at zero polarization, whereas the ferroelectric phase has multiple potential wells corresponding to nonzero polarization values and finite Ti ion displacements. In this picture, a long-range polarization develops spontaneously at the diffusionless phase transition due to the softening of a low-energy, transverse optical (TO) phonon mode. Despite the widespread use of the displacive model, experimental evidence of local structural distortions in the cubic, paraelectric phase of many ferroelectric perovskites [3–7] has led to proposals of alternative models, based on order-disorder transitions [3,8] or a combination of soft mode and order-disorder pictures [9,10]. In general, however, there exists no agreement in the literature about the nature of the displacements (static or dynamic) or the degree of correlations among them, both of which would be key to understanding the origin and the nature of ferroelectric transitions.

$SrTiO_3$ is an incipient ferroelectric [11] in its unstrained, pure bulk form, but easily becomes ferroelectric under small perturbations, such as mechanical stresses or alloying [12–15]. Understanding the nature of the ferroelectric transition of $SrTiO_3$ is important for many reasons. It is thought to be a prototype soft mode (incipient) ferroelectric [11,16,17]. As such, deviations from the classical Devonshire picture would likely have implications for other materials. The ferroelectric soft mode has also been suggested to play a role in the superconductivity of $SrTiO_3$ [18–23], whose Cooper pairing mechanism remains elusive despite several decades of research [24,25]. Recently, it was found that the superconducting transition temperature is doubled in compressively strained $SrTiO_3$ films [26,27] and ^{18}O-substituted $SrTiO_3$ crystals [28], for which a ferroelectric transition precedes the superconducting state upon cooling. Such "ferroelectric" superconductors have broken inversion symmetry [27], which, in conjunction with spin-orbit coupling, can give rise to unconventional superconductivity [29–34]. Ferroelectricity can thus potentially be used to tune the nature of the superconducting state of $SrTiO_3$.

Although the displacive model is generally used to describe the ferroelectric transition of $SrTiO_3$, indications of an order-disorder component have also emerged. For instance, signatures of polar clusters above the Curie temperature have been reported for ^{18}O-enriched $SrTiO_3$ and for $SrTiO_3$ containing impurities [6,7,35,36]. A low-temperature phase containing ordered ferroelectric regions has been suggested to exist even in pure, stress-free $SrTiO_3$ [37,38]. Recently, an Ising model was found to be the best descriptor of the temperature dependence of optical second harmonic generation (SHG) data near the ferroelectric phase transition of compressively strained $SrTiO_3$ films [27]. Such films also show a residual SHG signal in the paraelectric phase and one possible explanation is the existence of polar regions [27,39].

Images of polar regions above the Curie temperature of ferroelectric $SrTiO_3$ would provide the most direct evidence of an order-disorder transition. Atomic resolution high-angle annular dark-field imaging in scanning transmission electron microscopy (HAADF-STEM) is a powerful technique that is capable of determining the atomic column positions with picometer precision [40–43] and, consequently, should be able to detect regions that contain Ti columns that are off-centered from their nonpolar positions. Here, we use HAADF-STEM to measure static Ti-column displacement vectors at room temperature in the paraelectric phase of compressively strained $SrTiO_3$ films, which undergo a ferroelectric transition below 140 K

[26,27,44]. Unlike Ca-alloyed $SrTiO_3$, these films contain no large concentrations of alloying elements that could form defect clusters. Furthermore, the results can be directly compared with those of unstrained films grown under identical conditions that have identical defect and impurity concentrations, but do not become ferroelectric.

$SrTiO_3$ thin films were grown by hybrid molecular beam epitaxy (MBE) on (001) LSAT $[(LaAlO_3)_{0.3}(Sr_2AlTaO_6)_{0.7}]$ and (001) $SrTiO_3$ single crystals, respectively, as described elsewhere [45]. Oxygen and Ti were supplied via the metal-organic precursor, titanium tetra-isopropoxide [45]. The in-plane strain of films grown on LSAT is about -1% as long as the film thickness remains below the critical thickness for strain relaxation of about 180 nm [46]. High-resolution 2θ-ω x-ray diffraction scans of the samples are shown in the Supplemental Material [47]. These confirm an out-of-plane lattice parameter of 3.93 Å for $SrTiO_3$ films on LSAT, corresponding to a fully strained film. Interfaces are atomically abrupt with no extended defects (Fig. 1). As-grown films contain oxygen vacancies, which dope the films with about 4×10^{18} cm^{-3} charge carriers. Doped films grown on LSAT were previously shown to undergo a ferroelectric transition at low temperatures to a polar point group (4 mm) with the polar axis oriented normal to the film plane [27]. The ferroelectric transition temperature of the film studied here was about 140 K [47]. For comparison, a strain-relaxed and oxygen annealed film grown on LSAT was also investigated.

Cross-section TEM samples were prepared using focused ion beam milling with 2 keV Ga ions. STEM-HAADF was carried out using a Thermo-Scientific Talos G2 200 × S/TEM (C_s = 1.2 mm) at 200 keV with a semi-convergence angle of 10.5 mrad and a HAADF detector angular range of 48–200 mrad (camera length of 125 mm). To improve the signal-to-noise ratio, 20 images (2048 × 2048 pixels, 2 μ sec dwell time) were sequentially recorded and cross-correlated. Sample tilts can result in errors in the determination of column positions [48]. We used position averaged convergent beam diffraction (PACBED) [49] to reduce tilts to less than 1 mrad. Atomic column positions were obtained by iterative fitting to a two-dimensional Gaussian function to obtain picometer precision in the Ti column displacement measurements [42]. The Ti column displacement (polarization) vector was defined as the difference between the center of mass of the four surrounding Sr columns and the actual Ti-O column position obtained by 2D Gaussian fitting [see Fig. 1(d)]. All images were acquired at room temperature, well into the paraelectric phase, far above the ferroelectric phase transition.

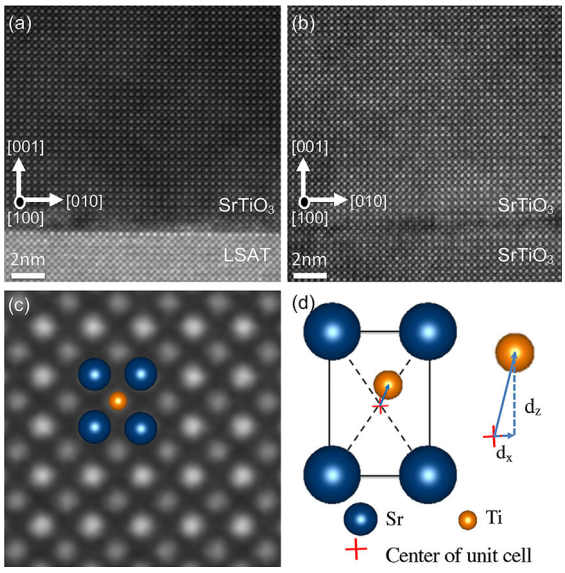

FIG. 1. Cross-section HAADF-STEM images of $SrTiO_3$ films grown on (a),(c) LSAT and (b) $SrTiO_3$. (d) A schematic illustrating the polarization vector and its components.

Figure 2 shows the polarization vectors for two representative images recorded from unstrained (left column) and strained (right column) $SrTiO_3$ films, respectively. The corresponding HAADF-STEM images and PACBED patterns can be found in the Supplemental Material [47]. The arrows in Figs. 2(a), 2(b) represent the directions of the polarization vectors and their magnitudes, which are also indicated by the color scale. The displacements in the unstrained film [Fig. 2(a)] are very small. As discussed in more detail below, they provide a measure of the experimental error (sample instabilities, image distortions, residual sample tilt) in determining the column positions

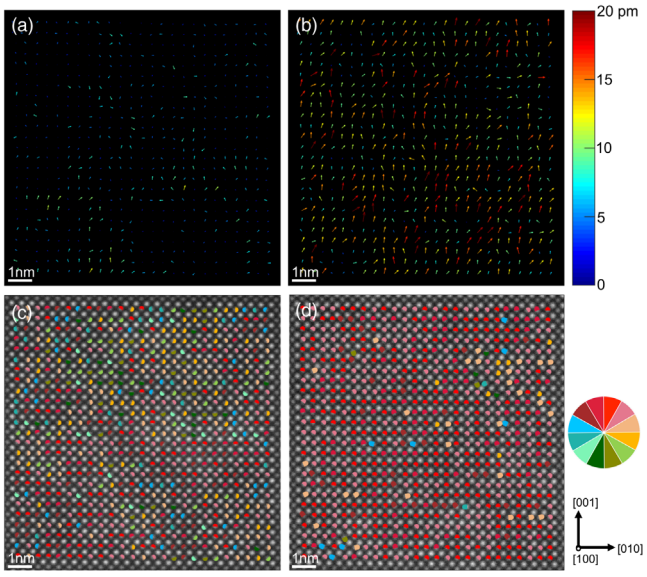

FIG. 2. Polarization vectors for $SrTiO_3$ films grown on (a), (c) $SrTiO_3$ and (b),(d) LSAT. The arrows in the figures in the top row indicate the magnitude (also indicated by the color scale) and orientation of the polarization vectors. The images in the bottom row display the direction of the polarization vectors overlaid on the HAADF image, with each color corresponding to a 30° interval of the polarization directions.

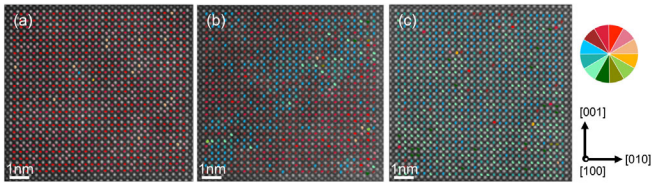

FIG. 3. Additional regions of the film on LSAT showing nanodomains of different polarization orientations. The colors indicate the direction of the polarization vectors, with each color corresponding to a 30° interval of the polarization directions. The colored dots are overlaid on the actual HAADF-STEM images. The corresponding polarization vectors are shown in the Supplemental Material [47].

and the influence of oxygen vacancies on the Ti-O columns. In contrast, the displacements in the strained film [Fig. 2(b)] are considerably larger. The average Ti column displacements relative to the center of the unit cell in these images are 4.2 ± 2.1 and 18.1 ± 7.4 pm for the unstrained and strained film, respectively. In addition, the films differ in the local alignments of their polarization vectors. Figures 2(c), 2(d) show their directions overlaid on the images. The color scale indicates the polarization orientation in 30° intervals. Note that the color scale indicates only the direction of Ti column displacements and is unconnected to their magnitude. The mostly random colors for the unstrained film [Fig. 2(c)] show that there is no preferential direction in the small Ti-column displacements. Despite the small displacements and their random orientation, there appears to be some degree of correlation between the displacements over a very small length scale of a few neighboring unit cells even in the unstrained film (see also additional images in the Supplemental Material [47]). In contrast, Fig. 2(d) is mostly populated by red color, which shows that the Ti column displacements in the strained $SrTiO_3$ film align along the growth direction in a region spanning many unit cells, forming a nanodomain.

Other areas of the strained film contain domains having different polarization directions (Fig. 3). For example, the Ti columns are displaced mostly along [001] in the image shown in Fig. 3(a), whereas in Fig. 3(c) they are displaced predominantly in-plane along $[0\bar{1}0]$. Figure 3(b) shows a region where a small $[0\bar{1}0]$ domain is surrounded by a [001] domain. Additional images of other polar domains and of nonpolar regions in both the unstrained and the strained films are shown in the Supplemental Material [47].

For better statistics and to understand the origins of the apparent small, random displacements in the unstrained sample, we analyzed a very large number of images. Figure 4 displays the results for the x and z components of the polarization vectors [defined in Fig. 1(d)] for unstrained and strained films and for the strain-relaxed, oxygen annealed film on LSAT. More than 10 000 Ti columns were analyzed for each sample. The displacements of the unstrained film on $SrTiO_3$ [Fig. 4(a)] have a Gaussian distribution with a full width at half maximum (FWHM) of 10 pm centered around zero displacement. In contrast, the strained film [Fig. 4(b)] shows bimodal distributions around nonzero values for each of the polarization components. The bimodal distribution can be more easily discerned for the in-plane (x) direction (see distribution on the top of the graph). Experimental error causes apparent canting of the polarization vectors, but some regions appear to have real displacements that (in the two-dimensional projection) are aligned along $\langle 011 \rangle$ [see also Fig. 2(b)]. The Ti column displacements of the strain-relaxed, oxygen annealed film are centered around zero, indicating no polar domains in this film, consistent with the absence of a ferroelectric transition. Interestingly, the distribution is narrower (FWHM of 8 pm) than for the unstrained film on $SrTiO_3$. We attribute this to the oxygen annealing, which removes the oxygen vacancies. Oxygen vacancies can cause small relaxations of the neighboring Ti columns immediately surrounding the columns [50,51]. Our results show that these displacements are random, unlike those of the polar nanodomains in the strained film. While the oxygen vacancies themselves do not produce a detectable change in the contrast of HAADF-STEM images, and their concentration is too low to be present with a high likelihood

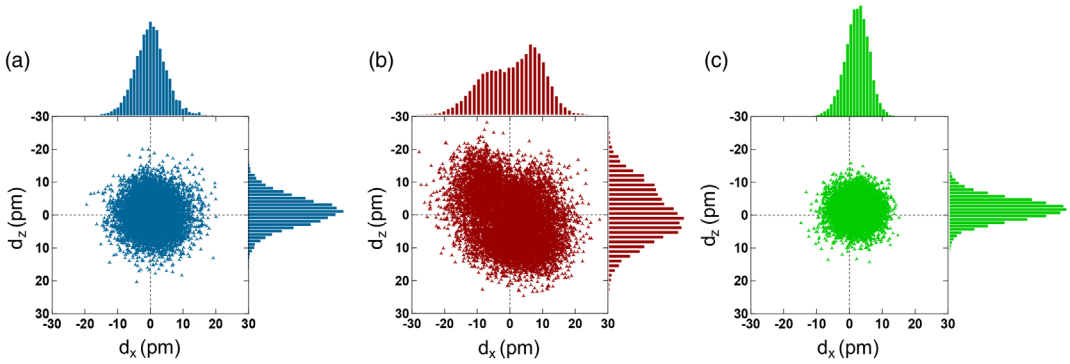

FIG. 4. Magnitude of displacement vector components [defined in Fig. 1(d)] acquired from multiple regions of films on (a) $SrTiO_3$, (b) LSAT, and (c) on LSAT after oxygen annealing.

in a single image, they can be detected in a statistical analysis of a large dataset of Ti column displacements.

To summarize, our observations of polar nanodomains at room temperature in the paraelectric phase of strained $SrTiO_3$, featuring correlated off-centering of Ti ions along the tetragonal axes, provide clear evidence in support of an order-disorder transition. A purely displacive transition would not exhibit Ti displacements in the paraelectric phase. The nanodomains only exist in films that subsequently undergo a ferroelectric transition at low temperatures, ruling out other possible proposed origins, such as impurities [7]. While the polarization is normal to the film plane throughout the entire film below the Curie temperature as a result of the compressive in-plane stress [27,39,47], significant fractions of the nanodomains have Ti displacements that are oriented in-plane, and some appear to be displaced/projected along $\langle 011 \rangle$. In the paraelectric phase, the different orientations and small size of the polar domains ensure that the fixed polarization charge in the domains remains compensated. This arrangement of nanodomains also makes the films appear nonpolar (or exhibit only a small remnant polarization) in global measurements, such as second harmonic generation, that average over many domains.

We next discuss the impact of our findings on the nature of the ferroelectric transition. Our observations of polar nanodomains in the paraelectric phase are consistent with a type of order-disorder transition originally proposed by Takahasi [8]. In particular, the fact that the displaced Ti ions form small ordered regions within which the displacements are correlated points to strong electrostatic interactions among the Ti ions already above the ferroelectric Curie temperature. This has several implications with regard to the nature of the phase transition. At the transition to the ferroelectric phase, in which the ferroelectric polarization is oriented globally out-of-plane, these existing dipoles must reorient, causing nanodomains to grow and percolate to form the long-range ordered state. The nature of the transition is therefore from a locally ordered, globally random phase to a globally ordered phase. The fact that the nanodomains exist above the transition temperature shows that the transition is driven by the strong electrostatic interactions of the Ti ions. Moreover, signatures of small, short-range correlated, but randomly oriented, displacements in the unstrained film point to interactions that exist to very high temperatures (relative to the phase transition temperature) and supports the possibility of earlier suggestions [37,38] of low temperature nanodomains even in unstrained, pure $SrTiO_3$. In other words, above the Curie temperature and with decreasing temperature, the interactions among neighboring unit cells become increasingly strong, causing the nanodomains to grow and the off-centering to develop along preferred orientations within a globally unpolarized, high-symmetry phase. The nanodomains are therefore an essential ingredient for the transition to take place.

It is also important to note that because of the long exposure time, HAADF-STEM images cannot detect dynamic polar fluctuations. Thus, our observations show static displacements within polar regions in the paraelectric phases. A dynamically disordered phase, which forms the basis for some of the theoretical proposals for $BaTiO_3$, would therefore be difficult to reconcile with our findings. We note the similarities with recent reports for $BaTiO_3$, which show static polar nanodomains [52,53] as well as static displacements in the cubic phase [54], and PbTe, which is close to a ferroelectric instability [55]. These similarities suggest that an order-disorder transition that is characterized by static, locally ordered dipoles in the paraelectric phase that transition to a long range ordered phase might be a more common feature than previously thought. The results have important consequences for modeling the ferroelectric transition of $SrTiO_3$, most of which were based on a displacive transition. Moreover, theories that link ferroelectricity to the superconductivity of $SrTiO_3$, especially those that connect the superconducting pairing mechanisms in $SrTiO_3$ to the soft mode behavior, should consider the complexity of the observed ferroelectric transition.

This work was supported by the U.S. Department of Energy (Grant No. DEFG02-02ER45994). Film growth experiments were supported by a MURI program of the Army Research Office (Grant No. W911NF-16-1-0361). This work made use of the MRL Shared Experimental Facilities, which are supported by the MRSEC Program of the U.S. National Science Foundation under Grant No. DMR 1720256.

*Corresponding author.
stemmer@mrl.ucsb.edu

[1] A. F. Devonshire, Philos. Mag. **40**, 1040 (1949).
[2] F. Jona and G. Shirane, *Ferroelectric Crystals* (Dover Publications, New York, 1993).
[3] R. Comès, M. Lambert, and A. Guinier, Acta Cryst. A **26**, 244 (1970).
[4] R. Comes, M. Lambert, and A. Guinier, Solid State Commun. **6**, 715 (1968).
[5] B. Ravel, E. A. Stern, R. I. Vedrinskii, and V. Kraizman, Ferroelectrics **206**, 407 (1998).
[6] B. Zalar, A. Lebar, J. Seliger, R. Blinc, V. V. Laguta, and M. Itoh, Phys. Rev. B **71**, 064107 (2005).
[7] H. Uwe, H. Yamaguchi, and T. Sakudo, Ferroelectrics **96**, 123 (1989).
[8] H. Takahashi, J. Phys. Soc. Jpn. **16**, 1685 (1961).
[9] Y. Girshberg and Y. Yacoby, Solid State Commun. **103**, 425 (1997).
[10] E. A. Stern, Phys. Rev. Lett. **93**, 037601 (2004).
[11] K. A. Müller and H. Burkard, Phys. Rev. B **19**, 3593 (1979).

[12] H. Uwe and T. Sakudo, Phys. Rev. B **13**, 271 (1976).
[13] J. G. Bednorz and K. A. Müller, Phys. Rev. Lett. **52**, 2289 (1984).
[14] M. Itoh, R. Wang, Y. Inaguma, T. Yamaguchi, Y. J. Shan, and T. Nakamura, Phys. Rev. Lett. **82**, 3540 (1999).
[15] J. H. Haeni, P. Irvin, W. Chang, R. Uecker, P. Reiche, Y. L. Li, S. Choudhury, W. Tian, M. E. Hawley, B. Craigo, A. K. Tagantsev, X. Q. Pan, S. K. Streiffer, L. Q. Chen, S. W. Kirchoefer, J. Levy, and D. G. Schlom, Nature (London) **430**, 758 (2004).
[16] Y. Yamada and G. Shirane, J. Phys. Soc. Jpn. **26**, 396 (1969).
[17] A. Yamanaka, M. Kataoka, Y. Inaba, K. Inoue, B. Hehlen, and E. Courtens, Europhys. Lett. **50**, 688 (2000).
[18] J. M. Edge, Y. Kedem, U. Aschauer, N. A. Spaldin, and A. V. Balatsky, Phys. Rev. Lett. **115**, 247002 (2015).
[19] K. Dunnett, A. Narayan, N. A. Spaldin, and A. V. Balatsky, Phys. Rev. B **97**, 144506 (2018).
[20] A. Stucky, G. W. Scheerer, Z. Ren, D. Jaccard, J. M. Poumirol, C. Barreteau, E. Giannini, and D. van der Marel, Sci. Rep. **6**, 37582 (2016).
[21] S. E. Rowley, C. Enderlein, J. F. d. Oliveira, D. A. Tompsett, E. B. Saitovitch, S. S. Saxena, and G. G. Lonzarich, arXiv:1801.08121.
[22] S. E. Rowley, L. J. Spalek, R. P. Smith, M. P. M. Dean, M. Itoh, J. F. Scott, G. G. Lonzarich, and S. S. Saxena, Nat. Phys. **10**, 367 (2014).
[23] C. W. Rischau, X. Lin, C. P. Grams, D. Finck, S. Harms, J. Engelmayer, T. Lorenz, Y. Gallais, B. Fauque, J. Hemberger, and K. Behnia, Nat. Phys. **13**, 643 (2017).
[24] C. Collignon, X. Lin, C. W. Rischau, B. Fauque, and K. Behnia, Annu. Rev. Condens. Matter Phys. **10**, 25 (2019).
[25] M. N. Gastiasoro, J. Ruhman, and R. M. Fernandes, Ann. Phys. (Amsterdam) **417**, 168107 (2020).
[26] K. Ahadi, L. Galletti, Y. Li, S. Salmani-Rezaie, W. Wu, and S. Stemmer, Sci. Adv. **5**, eaaw0120 (2019).
[27] R. Russell, N. Ratcliff, K. Ahadi, L. Y. Dong, S. Stemmer, and J. W. Harter, Phys. Rev. Mater. **3**, 091401 (2019).
[28] Y. Tomioka, N. Shirakawa, K. Shibuya, and I. H. Inoue, Nat. Commun. **10**, 738 (2019).
[29] V. Kozii and L. Fu, Phys. Rev. Lett. **115**, 207002 (2015).
[30] M. S. Scheurer and J. Schmalian, Nat. Commun. **6**, 6005 (2015).
[31] S. Kanasugi and Y. Yanase, Phys. Rev. B **98**, 024521 (2018).
[32] S. Kanasugi and Y. Yanase, Phys. Rev. B **100**, 094504 (2019).
[33] T. Schumann, L. Galletti, H. Jeong, K. Ahadi, W. M. Strickland, S. Salmani-Rezaie, and S. Stemmer, Phys. Rev. B **101**, 100503(R) (2020).
[34] K. Yada, S. Onari, Y. Tanaka, and J.-i. Inoue, Phys. Rev. B **80**, 140509(R) (2009).
[35] U. Bianchi, W. Kleemann, and J. G. Bednorz, J. Phys. Condes. Matter **6**, 1229 (1994).
[36] T. Shigenari, T. Nakano, and K. Abe, Europhys. Lett. **94**, 57001 (2011).
[37] K. A. Muller, W. Berlinger, and E. Tosatti, Z. Phys. B **84**, 277 (1991).
[38] E. K. H. Salje, O. Aktas, M. A. Carpenter, V. V. Laguta, and J. F. Scott, Phys. Rev. Lett. **111**, 247603 (2013).
[39] R. C. Haislmaier, R. Engel-Herbert, and V. Gopalan, Appl. Phys. Lett. **109**, 032901 (2016).
[40] A. B. Yankovich, B. Berkels, W. Dahmen, P. Binev, S. I. Sanchez, S. A. Bradley, A. Li, I. Szlufarska, and P. M. Voyles, Nat. Commun. **5**, 4155 (2014).
[41] X. H. Sang, E. D. Grimley, C. N. Niu, D. L. Irving, and J. M. LeBeau, Appl. Phys. Lett. **106**, 061913 (2015).
[42] H. Kim, J. Y. Zhang, S. Raghavan, and S. Stemmer, Phys. Rev. X **6**, 041063 (2016).
[43] S. Salmani-Rezaie, H. Kim, K. Ahadi, and S. Stemmer, Phys. Rev. Mater. **3**, 114404 (2019).
[44] A. Verma, S. Raghavan, S. Stemmer, and D. Jena, Appl. Phys. Lett. **107**, 192908 (2015).
[45] B. Jalan, R. Engel-Herbert, N. J. Wright, and S. Stemmer, J. Vac. Sci. Technol. A **27**, 461 (2009).
[46] T. Q. Wang, K. Ganguly, P. Marshall, P. Xu, and B. Jalan, Appl. Phys. Lett. **103**, 212904 (2013).
[47] See Supplemental Material at http://link.aps.org/supplemental/10.1103/PhysRevLett.125.087601 for x-ray diffraction results, the electrical resistance as a function of temperature for the strained film, PACBED and HAADF images of the regions analyzed in Fig. 2, the polarization vector maps for Fig. 3, and additional measurements of the polarization vectors in different regions of the strained and unstrained samples and at low temperature.
[48] P. Gao, A. Kumamoto, R. Ishikawa, N. Lugg, N. Shibata, and Y. Ikuhara, Ultramicroscopy **184**, 177 (2018).
[49] J. M. LeBeau, S. D. Findlay, L. J. Allen, and S. Stemmer, Ultramicroscopy **110**, 118 (2010).
[50] M. O. Selme and P. Pecheur, J. Phys. C **16**, 2559 (1983).
[51] C. Mitra, C. Lin, J. Robertson, and A. A. Demkov, Phys. Rev. B **86**, 155105 (2012).
[52] Y.-T. Shao and J.-M. Zuo, Acta Cryst. B **73**, 708 (2017).
[53] K. Tsuda and M. Tanaka, Appl. Phys. Express **9**, 071501 (2016).
[54] T. Nakatani, A. Yoshiasa, A. Nakatsuka, T. Hiratoko, T. Mashimo, M. Okube, and S. Sasaki, Acta Crystallogr. B **72**, 151 (2016).
[55] B. Sangiorgio, E. S. Bozin, C. D. Malliakas, M. Fechner, A. Simonov, M. G. Kanatzidis, S. J. L. Billinge, N. A. Spaldin, and T. Weber, Phys. Rev. Mater. **2**, 085402 (2018).